OBȚINEREA ȘI PROPRIETĂȚILE GAZOBETONULUI CU ADAOS DE STERIL CU CONȚINUT DE ZINC ȘI PLUMB

PREPARATION AND PROPERTIES OF AUTOCLAVED AERATED CONCRETE CONTAINING LEAD-ZINC TAILINGS

GENG LIN[1], CHANG-LONG WANG[2, 3*] , CHUN-YU QIAO[4], HAN-LONG CUI[3], LIE CHEN[3], SHUO YU[5]

[1]*School of Chemistry and Chemical Engineering, Xi'an University of Science and Technology, Xi'an Shaanxi Province, 710054, China.*

[2]*School of Resources and Environmental Engineering, Jiangxi University of Science and Technology, Ganzhou Jiangxi Province, 341000, China.*

[3]*School of Civil Engineering, Hebei University of Engineering, Handan Hebei Province, 056038, China.*

[4]*State Key Laboratory of High-Efficiency Mining and Safety of Metal Mines, University of Science and Technology Beijing, Ministry of Education, Beijing 100083, China.*

[5]*The Third branch, Tianjin Engineering and Construction Corporation, Tianjin 300384, China.*

To comprehensively utilize lead-zinc tailings (LZT), it was used as main siliceous materials in autoclaved aerated concrete (ACC) in this study. The effects of fineness and content of LZT on the properties, hydration products and microstructures of AAC were investigated by the mechanical test, X-ray diffraction analysis (XRD), Fourier transform infrared spectroscopy (FT-IR), thermogravimetric/differential scanning calorimeter (TG-DSC) and scanning electron microscope (SEM). And the composition and morphology of the hydration products in AAC at varying stages were detected. The results show that the ACC containing 62% LZT (in mass percentage) with a specific surface area of 325 m^2 kg^{-1} can achieve a bulk density of 587 kg m^{-3} and compressive strength of 4.94 MPa, which qualifies the requirements of A3.5, B06 level of AAC sample regulated by the composition and morphology GB/T 11969-2008. The mobility of slurry and hydration activity both increase as the fineness of LZT decreases. However, the small size of LZT particles and the high thickness of the slurry are harmful to form a good pore structure, which would influence the properties of AAC. When the blending percentage of LTZ is too high, the unreacted LTZ particles increase and accumulate within the system, which reduces the space among them and thus influences the growth and crystallization of hydration products. The main hydration products before curing are AFt and C-S-H gels. And then AFt decomposes and some amount of C-S-H transitions to tobermorite after curing and autoclaved.

Keywords: *lead-zinc tailings, autoclaved aerated concrete, fineness, content, tobermorite*

1. Introduction

Lead-zinc tailings (LZT) is one kind of main industrial solid wastes in China, and it can be obtained from the dehydrated ore pulp during ore sorting [1,2]. LZT is a concomitant mine with various heavy metals, non-metallic minerals and other hazardous substances. The metal components in LZT are difficult to recycle and thus the plants usually store LZT by stockpiling, which occupies a large amount of arable land, causes serious pollution to the surrounding environment and severely affects the local sustainable development [3-7]. After crushing, grinding and milling, the obtained fine LZT particles contain a large amount of silicate minerals, and it has different physical and chemical properties compared with the conventional raw materials, such as fly ash and river sand, used in autoclaved aerated concrete [8,9]. The active components in silicate minerals, such as Al_2O_3 and SiO_2, are prone to hydrate in an alkaline hydrothermal environment at high temperature and high pressure, and form calcium silicate hydrates (C-S-H) [10-13]. Iron ore tailings containing silicate minerals have been successfully applied in AAC production in China. Furthermore, copper tailings, phosphorus tailings and other tailings also show promising potentials to be utilized in AAC industry [14-16]. Zhang [17] and Chen and Li et al. [18] studied the production of B05, B06 level AAC with LZT. However, the content of LZT in their studies was little and analysis on the reaction mechanism of LZT was not carried out. In this paper, LZT will be used as the main raw material in AAC with as little amount of cement. The effects of fineness and content of LZT on AAC properties will be analyzed using XRD, FT-IR, TG-DSC and FE-SEM. And the hydration products and microstructure within AAC will be analyzed as well.

2. Materials and Methods

2.1. Experimental materials

The AAC samples were prepared using the following raw materials: LZT, lime, P·O 42.5 Portland cement and desulphurisation gypsum.

Portland cement. The initial and final setting times of the P·O 42.5 Portland cement are 107 min and 182 min, respectively.

LZT. The chemical compositions of LZT (mass fraction, similarly hereinafter) are shown in Table 1

* Autor corespondent/*Corresponding author*,
E-mail: 13716996653@139.com

Table 1

Chemical composition of raw materials (mass fraction, %)

Materials	SiO_2	Al_2O_3	Fe_2O_3	FeO	CaO	MgO	Na_2O	K_2O	SO_3	MnO	Loss
LZT	66.23	7.67	2.45	3.12	8.51	1.78	0.54	0.65	—	4.13	3.83
Lime	4.79	4.32	3.21	0.48	76.89	2.96	—	1.63	0.53	—	4.18
Cement	26.12	5.75	3.17	0.93	57.29	1.53	0.54	0.31	—	0.12	4.02
Desulfurization gypsum	2.64	0.84	0.08	0.22	43.65	0.14	0.21	0.23	31.16	—	—

and the content of SiO_2 is 66.23 %. Leaching toxicity of heavy metals in LZT is qualified according to Chinese standard GB/T 5085.3—2007 as well as its radioactivity according to Chinese Standard 6566-2010. The 0.08 mm sieve residue of LZT was 66.41%.

Lime. The composition of lime is shown in Table 1and the content of effective CaO is 71%. Its digestion time is 12 min, and the digestion temperature is 67 ºC according to Chinese standard JC/T621-1996. And 0.08 mm sieve residue is less than 15%.

Desulphurisation gypsum. The specific surface area of the desulphurisation gypsum is 389 $m^2 kg^{-1}$. Its chemical compositions are listed in Table 1, and 0.08 mm sieve residue is less than 7.9%.

Other materials. Aluminum powder paste in oil was used as the foaming agent using and the foam stabilizer is a specific mixture of oleic acid, triethanolamine and water at room temperature.

2.2. Experimental Method

2.2.1. Preparation of AAC

Firstly, LZT was dried until its moisture was less than 1%. Then, small laboratory ball mill (SM φ 500 mm × 500 mm) was used to grind it into powder. The relationship between the grinding time and the specific surface area is shown in Figure 1.

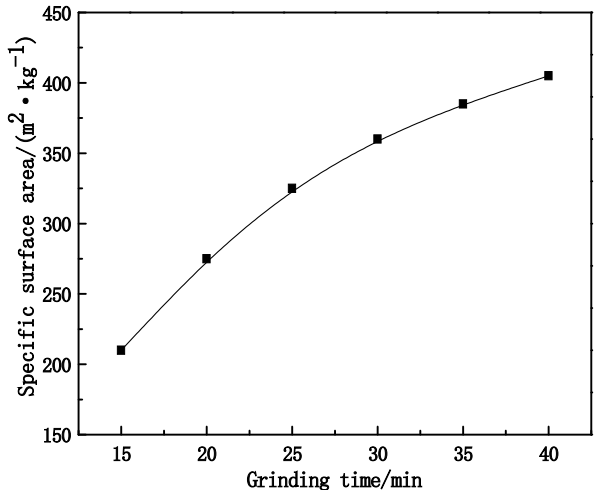

Fig.1 - Relationship between the grinding time and the specific surface area of LZT.

(1) Preparation of AAC containing LZT with varying fineness

The amounts of LZT, cement, quicklime, gypsum are 1320 g, 550 g, 220 g, 110 g, respectively. And the amounts of water, aluminum paste and foam stabilizer are 1254 g, 1.32 g and 0.56 g, respectively.

The dry mixtures were stirred in warm water (50 ºC) for 120 s; then added aluminum paste and foam stabilizer and continued to stir the mixtures for 40s. The slurry was poured into the triple-mold molds (100mm×100mm×100mm), then cured at 60 ºC for 4 h. After de-molded, the hardened slurries were autoclaved for 8 h (the highest pressure is 1.25 MPa, and the highest temperature 185 ºC). The different LZT fineness of AAC samples were labeled as Z1~Z6.

(2) The preparation of AAC with different amounts of LZT

LZT with the optimal fineness was used and its blend amounts are as follows: 1188 g, 1232 g, 1276 g, 1320 g, 1364 g, 1408 g and 1452 g. These different LZT contents of AAC samples were labeled as C1~C6 . The amounts of water, aluminum powder pastes and foam stabilizer were the same as before.

2.2.2. Sample characterisation

The bulk density and compressive strength of the AAC samples were measured according to Chinese standard GB/T 11968-2008. For bulk density measurements, three samples of each AAC mixture were oven dried at 60 ± 5 ºC for 24 h, then at 80 ± 5 ºC for 24 h, and finally at 105 ± 5 ºC for 24 h, consecutively. The mass of the oven dried samples was used to calculate the bulk density.

The X-ray diffraction (XRD) spectra analysis of AAC samples was carried out using a D/Max-RC diffractometer (Japan) with Cu Kα radiation, voltage of 40 kV, current of 150 mA and 2θ scanning ranging between 5 º and 90 º. The functional groups vibration of each sample was qualitatively analyzed by NEXUS70 Fourier transform infrared (FT-IR, test range 350~4000 cm^{-1}). The DSC-TG analysis of the AAC samples was performed from 20 to 1000 ºC at a rate of 10 ºC/min using a Netzsch STA 449C thermal analyser with dry air as the stripping gas. FESEM observation was performed to analyse the hydration products of the AAC samples using a

Zeiss SUPRA^{TM}55 scanning electron microscope coupled with a Be4-U92 energy spectrum.

3. Results and Discussion

3.1. Effect of the fineness of LZT on AAC properties

The original LZT used herein is not activity, so efforts must be taken to increase the activity before used in AAC. The activation energy of the material decreases through mechanochemical effect [19-21]. The mechanical activated power helps decrease the particle size of raw material and increase the specific surface area, which leads to increase the surface free energy and reactivity [22, 23]. Thus, the ground siliceous materials played a role not only in physical filling, but also in chemical reaction to form the main hydration products in AAC. The fineness of siliceous material is the key factor during AAC production. The particle size distribution of the siliceous raw material directly affects its reactivity and the pouring stability of slurry.

Fig. 2 shows the relationship between LZT fineness and properties of AAC. It indicates that the compressive strength of AAC samples increases firstly and then decreases as the fineness of LZT increases, while its dry bulk density tends to decrease first and then to increase. Bulk density of all six groups is smaller than 625 kg m^{-3}, which meet the requirement of Chinese standard B05 AAC . And the compressive strength of Z2, Z3, Z4, Z5, Z6 samples is all higher than 3.5 MPa, which meet the requirement of Chinese standard A3.5 AAC. Thus, the fineness of lead-zinc tailing is critical for AAC properties. The increased fineness of LZT helps enlarge its surface area in contact with water. The newly increased surface by grinding is supposed to make LZT more amorphous, which is beneficial in improving its rate of dissolution and enhancing its participation in chemical. Slight bubbling phenomenon was observed when the Z6 sample with specific surface area of 405 m^2 kg^{-1} was cast. Moreover, the fresh slurry of Z6 is very viscous and the hardened Z6 AAC sample appears micro-and meso-cracks. All above indicates that the smaller fineness and larger surface area of LZT help achieve the higher the activity and the better slurry flow. However, when the LZT fineness is too small, the viscous slurry is harmful in forming a good pore structure and in improving AAC properties. Z1 sample with a specific surface area of 207 m^2 kg^{-1} shows poor slurry fluidity and bubbling phenomenon, which suggests that coarse LZT tailings may result in poor fluidity. And its settlement becomes fast after casting and it leads to the collapse of the slurries. The experimental results show that the fluidity and pouring stability of the slurry are good when specific surface area of LZT is 325 m^2 kg^{-1}. And the bulk density and compressive strength of samples are optimal and it has the best

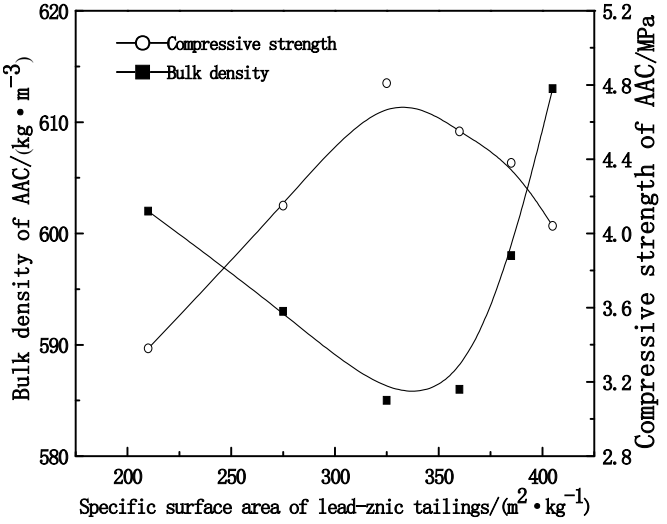

Fig. 2 - Influence of fineness of lead-zinc on AAC samples properties.

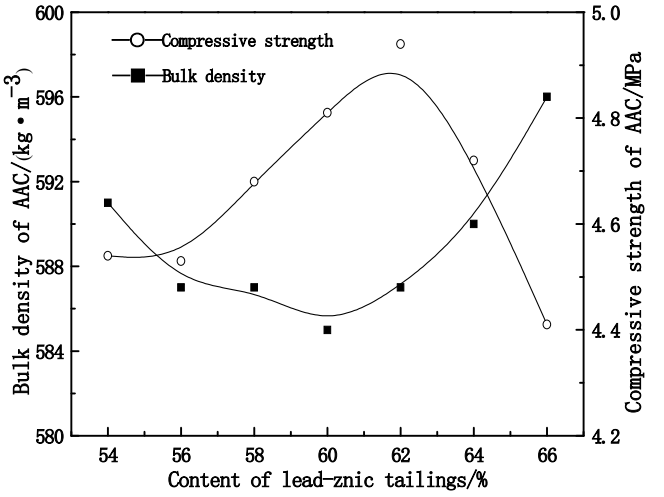

Fig. 3 - Influence of LZT content on AAC samples properties

appearance. Therefore, the optimal specific surface area of the following test tailings 325 m^2 kg^{-1}.

3.2. Effect of the content of LZT on AAC properties

Fig. 3 shows the influence of LZT content on AAC samples properties. It indicates that compressive strength of AAC samples tends to increase firstly and then decrease, and the absolute dry density tends to decrease firstly and then increase when increasing the LZT content. In addition, the amount of dissolved active SiO_2 and Al_2O_3 increases during autoclaving. And the hydration reaction tends to complete, and the crystal morphology of hydration products (tobermorite) tends to be good, hydration products combines more closely with unreacted particles in the system, which leads to the increase of the compressive strength of AAC samples and decrease of the bulk density, but when mixing with excessive LZT, residual unreacted particles of

tailing in the system increases, the space among the particles reduces, which restrains the growth and crystallization of hydrates[24, 25]. Thus, the compressive strength of AAC samples reduces and their bulk density increases. When the LZT content is 64% or 66%, the excessive LZT decreases the slurry fluidity, the initial consistency of the slurry increases, pore structure non-uniform pore inside body, expanded height of body decrease, the compressive strength reduce and the pore structure of hydration products uneven. When the content of LZT is 66% (C7 sample), tiny flaws in the vertical direction can be observed on the outer surface of sample, which indicates that the LTZ content could not be larger than 62% under the experimental scenarios and when the LTZ content is 62%, the absolute dry density of sample is 587 kg m^{-3} and the compressive strength could reach 4.94 MPa. For the purpose of utilizing as large amount of LZT as possible, C7 is optimal with LZT of 62%, lime of 24%, cement of 9% and desulfurization gypsum of 5%.

3.3. XRD analysis

In order to verify the reliability of C5 mixture proportion, the XRD test results of C5 samples before and after autoclaved are shown in Fig.4. It shows that the main mineral compositions of LZT include quartz (SiO_2), hedenbergite ($CaFe(Si_2O_6)$), calcium manganese pyroxene ($CaMn(SiO_3)_2$), calcite ($CaCO_3$), diopside ($CaMg(Si_2O_6)$) and epidote ($Ca_2FeAl_2[SIO_4][SI_2O_7]O(OH$)). Compared with the original LZT, newly formed ettringite and $Ca(OH)_2$ (portlandite) could be observed, and the main XRD diffraction peaks of mineral composition of the original LZT decreases. Among them, $Ca(OH)_2$ forms due to cement hydration and lime digestion while the formation of ettringite mainly come from two parts. One is that hydration calcium aluminate (C-A-H) that reacts with SO_4^{2-} in gypsum to form ettringite (AFt). The other is that the ultrafine particles in LZT partly reacts with $Ca(OH)_2$ to form hydrated calcium silicate (C-S-H gels) and hydrated calcium aluminate crystals. Ettringite crystal rapidly forms from the reaction of hydrated calcium aluminate with gypsum, which may be the reason that the intensity quartz diffraction peaks in the curve 2 reduces. At the same time, the broad halo in the two theta range between 26 ° and 34 ° suggests that there is amorphous diffraction (no) of amorphous and low crystallized C-S-H [24].

X-ray diffraction (XRD) is used to analyze the mineral phases of LZT and sample C5 before and after autoclaved, and the test results are presented in Fig.4.

The comparison between curve 2 and curve 3 indicates that tobermorite and anhydrite newly form, the diffraction peak of ettringite and $Ca(OH)_2$ disappear, and the quartz diffraction peak intensity further reduces in the hardened sample after curing for 2 h at 70 ºC. This may be mainly due to that in the process of, the dissolution rate of SiO_2 and Al_2O_3 in LZT accelerates and more SiO_2 and Al_2O_3 components reacts with $Ca(OH)_2$ to form hydration products (such as C-S-H gels and hydrated calcium aluminate crystal) during curing. As the amount of dissolved SiO_2 increases, the Ca/Si ratio in the fluid decreases and C-S-H forms at the initial cement hydration stage. And $Ca(OH)_2$ can react with SiO_2 gel to form weakly alkaline C-S-H and tobermorite. Ettringite could decompose into AFm, Al^{3+} and SO_4^{2-} at high temparature [26-28]. AFm continues to decompose into C_3AH_6 and $CaSO_4$ during curing, so there are no ettringite diffraction peaks in curve

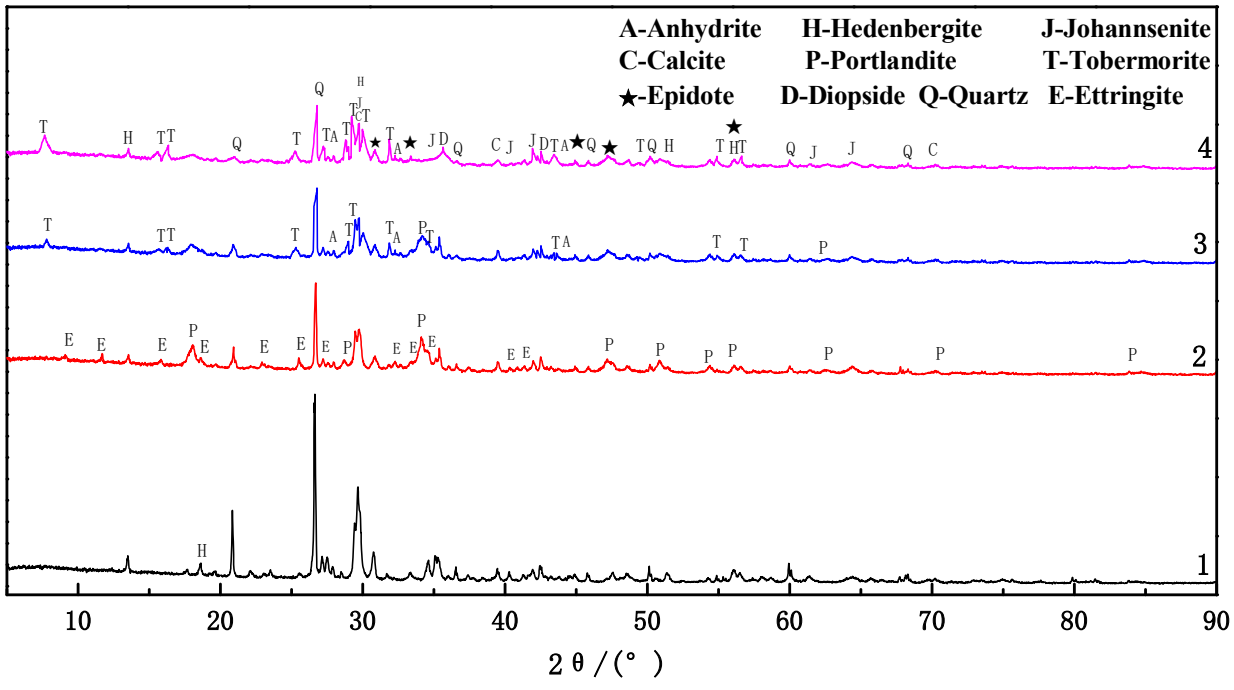

Fig. 4 - XRD spectrums of C5 AAC samples and LZT. 1-LZT, 2- body before curing, 3- body after curing, 4- sample after autoclaved

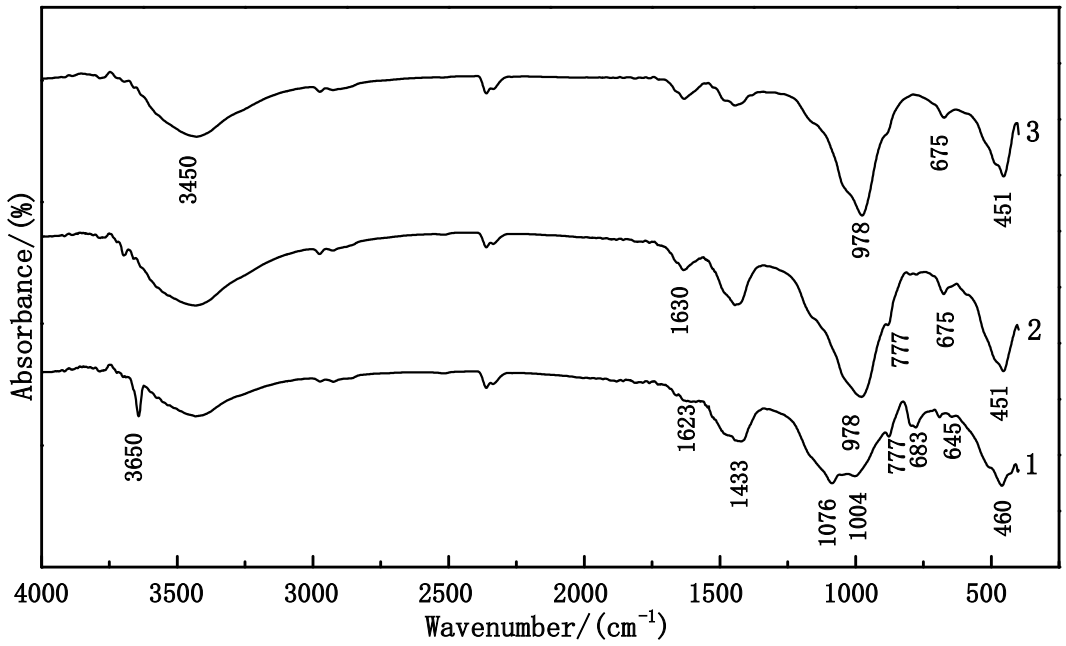

Fig. 5 - FT-IR spectrums of C5 AAC samples: 1- body before curig, 2- body after curing, 3- sample after autoclaved

3 after curing for 2 h at 70 ºC. And diffraction peak intensity of the gypsum in curve 3 is strengthened after curing due to the delayed coagulation of gypsum and decomposition of AFm.

3.4. FT-IR analysis

Fig.5 shows FT-IR spectrums of the C5 samples before curing, after curing and after autoclaved. As shown, the absorption peaks move towards lower wave-numbers. In curve 1 for C5 before curing, the strongest absorption region 1250~1100 cm^{-1}, the weak band 1160~1250cm^{-1} and the strong band 1076~1100 cm^{-1}, belong to the absorption band of quartz and related to anti-symmetric stretching mode of Si-O, respectively. The absorption bands at 1076, 777 and 460 cm^{-1} can be attributed to anti-symmetric stretching mode of Si-O, symmetric stretching mode of Si-O-Si, bending mode of Si-O, respectively [29]. Wavenumber around 3650 cm^{-1} absorption band is the result of Ca $(OH)_2$ stretching vibration of the hydroxyl group. Wavenumber characteristic peak at 3450 cm^{-1} comes from stretching vibration of the adsorbed water in C-S-H gels and AFt. Bending vibration wave number at about 1623cm^{-1} absorption band is attributed to hydroxyl in the absorbed water in C-S-H and AFt. Asymmetric stretching vibration absorption bands in the wave number at 1433cm^{-1} belongs to CO_3^{2-} in calcite due to carbonization. Wavenumber in the broader band 1000cm^{-1} ~ 1050cm^{-1} can be attributed to the stretching vibration around Si-O bond in C-S-H. Wavenumber in 640 ~ 700 cm^{-1} is characterized as O-Si (Al) -O bending vibration, which belongs to the vibration bands of pyroxene in LZT.

In Fig.5, curve 3 belonging to C5 sample after autoclaved is similar to curve 2 of hardening C5 sample after curing for 2h. However, the characteristic bands of quartz group minerals at 1076, 1004, 683, 645 and 460 cm^{-1} disappear, which suggests that the amount of formed hydration products increases after autoclaved and they tend to crystalize. The decomposition of AFt at high temperatures is confirmed by the disappearance of absorption band at 1623cm^{-1} belonging to ettringite in curve 3. Meanwhile new characteristic peaks at 1630cm^{-1}, 978m^{-1} and 451cm^{-1} observed are related to the bending mode in H_2O in curve 2 and 3, the symmetric stretching mode of Si-O in $[SiO_4]$ structure Q^2, and the bending mode of Si-O, respectively. The strong infrared band of stretching vibration of Si-O lead to high intensity band at 978m^{-1}, which together with 451cm^{-1} is attributed to the layered structure of tobermorite.

3.5. TG-DSC analysis

Fig 6(1)-(3) are TG-DSC profiles of AAC samples before curing, after curing and after autoclaved for 12 h, respectively. As shown in Fig 6, a broad endothermic peak exists in the range of 80~200 ºC, which can be attributed to the dehydration of AFt and C-S-H [30].

There are varying endothermic peaks at 107 ºC, 463 ºC, 577 ºC and 762 ºC, as indicated in Fig 6(1). There is a mass loss of 4.38% belonging to the relatively sharp endothermic peak at 107 ºC, which results from the dehydration of AFt. The endothermic peak at 463 ºC is the outcome of the decomposition of $Ca(OH)_2$. The endothermic peak at 577 ºC mainly suggests the transition of β-quartz

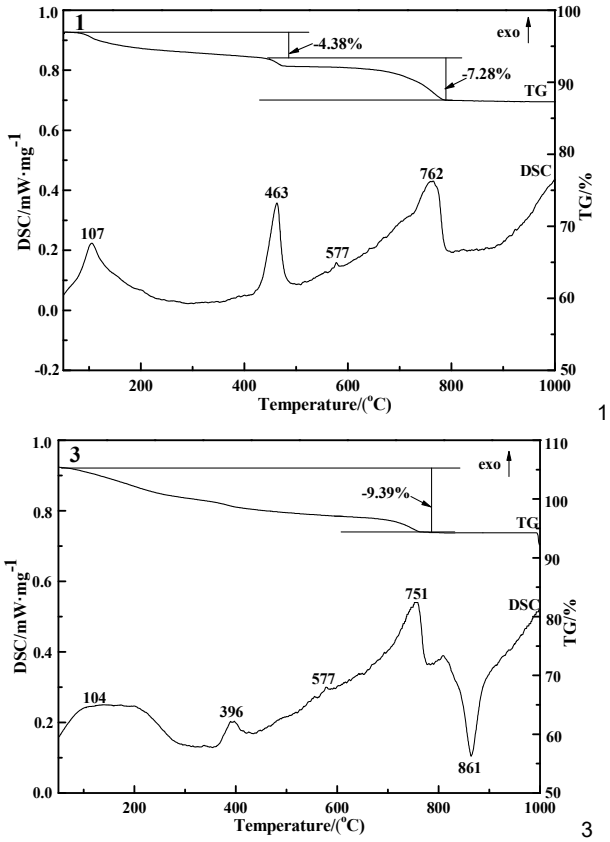

Fig. 6 - TG-DSC spectrums of C5 AAC samples. 1- body before curing, 2- body after curing, 3- sample after autoclaved

to α-quartz [31] in the lead-zinc ore tailings while no mass loos is obtained in TG profile. And the endothermic peak at 762 ºC is supposed to be caused by the dihydroxylation of C-S-H as well as the decomposition of calcite.

In Fig 6(2), dehydration of ettringite results in the endothermic peak at 114 ºC while dehydration of gypsum contributes to the one at 114 ºC. The lower intensity of the endothermic peak at 460 ºC in Fig 6(2), compared with the one in Fig 6(1), may result from the consumption of $Ca(OH)_2$ via its reaction with activated SiO_2 and Al_2O_3 in lead-zinc ore tailings during curing. The analysis is in consistence of the XRD and FTIR analysis.

The TG-DSC research by Klimesch et al. [32] shows that C-S-H can transition to okenite via dihydroxylation at 840 ºC~900 ºC and the transition temperature increases as the amount of Al^{3+} in C-S-H increases. Thus, the exothermic peak at 861 ºC is the result of the transition of Al-tobermorite, which is the main reaction products in AAC samples. And it should be noticed that there is no endothermic peak belonging to the dehydration of $Ca(OH)_2$ and this indicates its entire consumption via reaction during autoclaving, which is in consistence with the XRD and FTIR analysis.

3.6. FE-SEM analysis

Fig. 7 and Fig. 8 illustrate FE-SEM and EDS of C5 samples before curing, after curing and after autoclaved. As shown in Fig. 7 (a) and (a1), the main hydration products in C5 sample before curing include poor crystallized C-S-H and needle-shaped AFt, and the observation is in accordance with with the XRD analysis. The spectroscopy of marked region 1 in Fig. 7 (a1) shows that the main elements in that area are Ca, S and Al, which are the same as AFt. C-S-H mainly forms due to the hydration of cement in AAC while AFt forms due to the reaction of gypsum and calcium aluminate hydrates. Fig.7 (b) and (b1) show the microstructure of C5 sample after the curing for 4 h. C-S-H with a high degree of crystallinity and plate-shaped hydrates can be observed. The EDS spectrum of region 2 in Fig. 7 (b) shows that Al exists in the plate-shaped hydrates due to the partial substitution of $[SiO_4]$ by $[AlO_4]$ [33]. Hydration products in the area 2 $nCa/n(Si+Al) = 0.8326$ can be obtained, which is the same as that of tobermorite $(Ca_5(OH)_2Si_6O_{16}!4H_2O)$ $n(Ca)/n(Si) = 0.8333$. AFt cannot be found in Fig. 7 (b) and (b1), which may suggest that AFt may decompose during curing for 4 h at 60 ºC [27]. And this is consistent with the FT-IR analysis in Fig. 4.

Fig.7(c) shows the hydration products in AAC after autoclaved for 12 h, which are mainly tobermorite and C-S-H. A large amount of plate-shaped tobermorite with the thickness of about 0.1 ~ 0.2 μm can be observed in Fig.7 (c1). The crystallinity of plate-shaped tobermorite increases greatly after autoclaved, and they intertwine together to forming the skeleton structure of AAC products, which contributes to the strength of AAC. After autoclaved, the solubility of active SiO_2 and Al_2O_3 in LZT increased in alkaline water heat

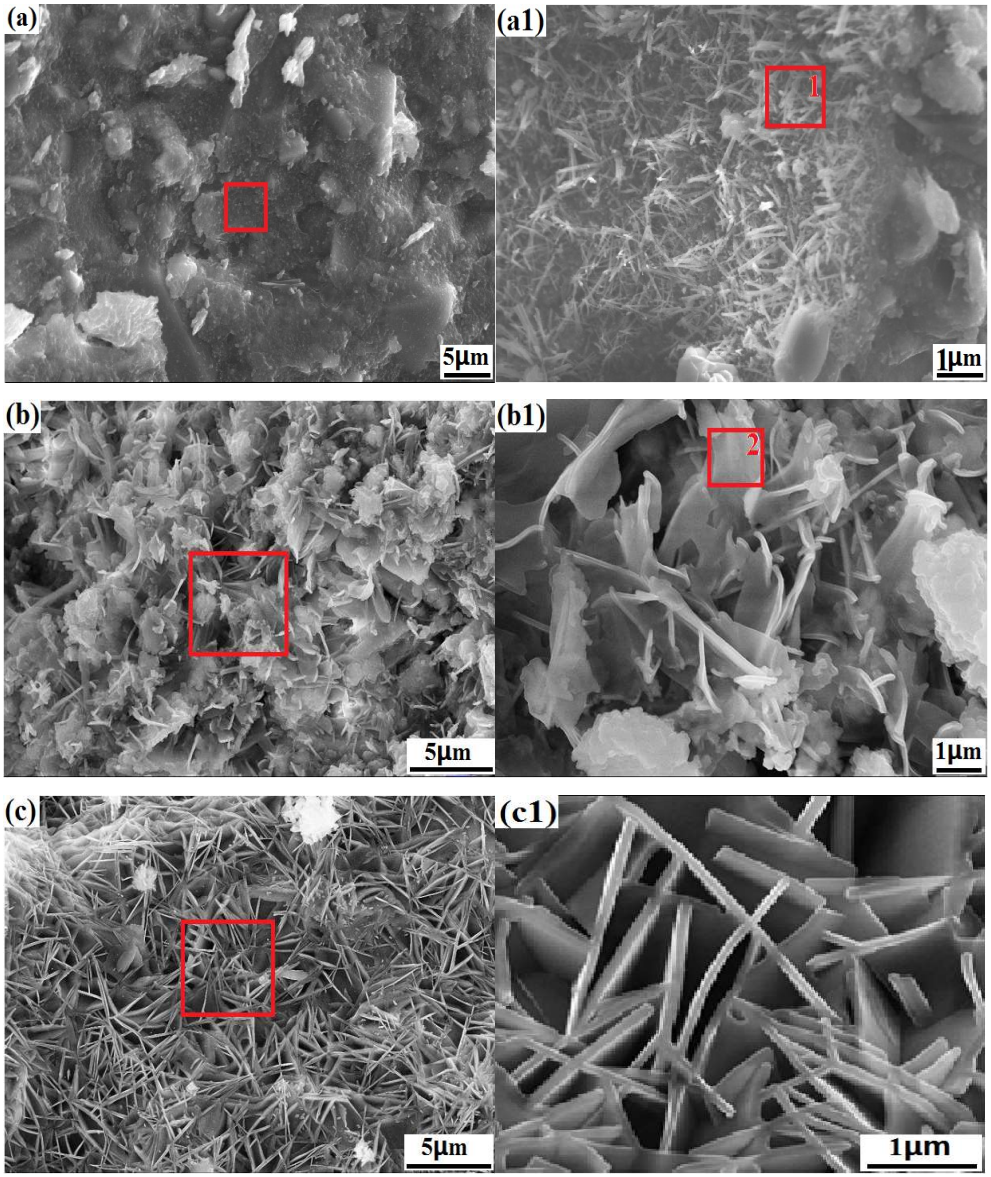

Fig. 7 - FE-SEM micrographs of C5 AAC samples. **(a) and (a1)**- body before curing, **(b) and (b1)**- body after curing, **(c) and (c1)**- sample after autoclaved.

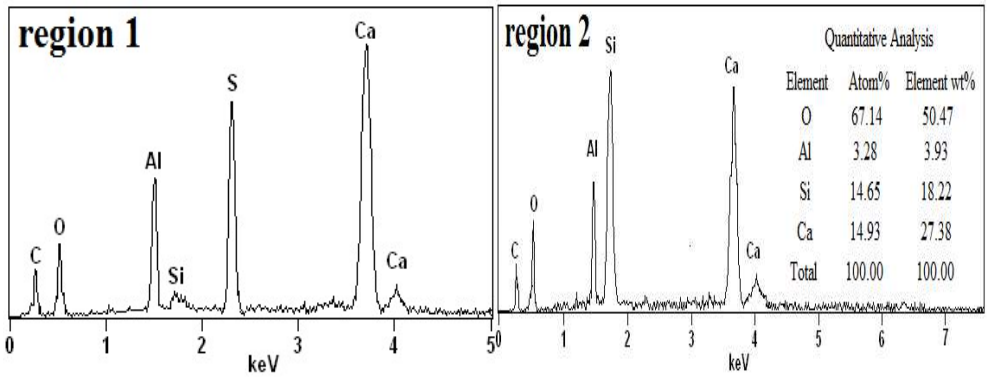

Fig. 8 - The EDS spectrums of marked region 1 and 2 in the Fig. 7.

environment and ability to participate in chemical reactions enhanced, which played a positive role in improving the crystallinity of hydration products.

4. Conclusions

(1) Qualified AAC with A3.5, B06 level according to Chinese standard GB/T 11968-2008 could be prepared with LZT as the main raw material.

(2) As the LZT fineness decreases, the stability of fresh slurry and physical mechanical properties of AAC samples are enhanced, but too small size of LZT grains would lead to deterioration of corresponding physical properties. The decreased fineness of LZT is advantageous for increase its surface area in contact with water, which improves the rate of dissolution and enhances its participation in the chemical reaction. Thus, the strength of the samples is improved. However, when the size was too small and the slurry is viscous, AAC samples the properties and pore structure would be affected.

(3) As the LZT content increases, the amount of dissolved active SiO_2 and Al_2O_3 increases in the system, and the hydration reaction tends to complete. Thus, the physical and mechanical properties of AAC samples enhances. But when mixing with excessive LZT, residual and the amount of unreacted LZT increases in the system. The space among the particles reduces, which restrains the growth and crystallization of hydration products, resulting in the degradation of products.

(4) Hydration products of body before curing mainly includes AFt and C-S-H gels; After curing, hydration products contain a large amount of tobermorite and C-S-H gels with higher crystallinity; after autoclaved, the ability of the activate components of LZT, such as SiO_2 and Al_2O_3, to participate in the chemical reaction enhances and the crystallization degree of tobermorite improves.

Acknowledgments

The authors gratefully acknowledge financial support from the National Key Technology R&D Program (2014BAE05B00), China Postdoctoral Science Foundation (2015T80095, 2015M580106), Natural Science Foundation of Hebei Province (E2015402057), supported by State Key Laboratory of Solid Waste Reuse for Building Materials (SWR-2014-007), supported by science and technology research project of higher education universities in Hebei Province (ZD2016014),supported by Comprehensive Utilization of Tailing Resources Key Laboratory of Shaanxi Province (2014SKY-WK010), Construction Science and Technology Foundation of Hebei Province (2012-136).

REFERENCES

1. W.S. Shu, Z.H. Ye, C.Y. Lan, Z.Q. Zhang and M.H. Wong, Acidification of lead-zinc mine tailings and its effect on heavy metal mobility, Environment International, 2001, 26(5-6), 389.
2. Y.P. Wang, PhD thesis, Empirical study of system management of lead-zinc tailings in Shaoxing Yinshanfan, Hangzhou Dianzi University, China, 2011.
3. H.B. Zhang, W. Shi, M.X. Yang, T. Sha and Z.W. Zhao, Bacterial diversity at different depths in Lead-zinc mine tailings as revealed by 16S rRNA gene libraries, The Journal of Microbiology, 2007, **45**(6), 479.
4. L.W. Titshall, J.C. Hughes and H.C. Bester, Characterisation of alkaline tailings from a lead/zinc mine in South Africa and evaluation of their revegetation potential using five indigenous grass species, South African Journal of Plant and Soil, 2013, **30**(2), 97.
5. Z.H. Ye, W.S. Shu, Z.Q. Zhang, C.Y. Lan and M.H. Wong, Evaluation of major constraints to revegetation of lead/zinc mine tailings using bioassay techniques, Chemosphere, 2002, **47**(10), 1103.
6. S.H. Yin, A.H. Wu, K.J. Hu, Y. Wang and Y.K. Zhang, The effect of solid components on the rheological and mechanical properties of cemented paste backfill, Minerals Engineering, 2012, **35**(6), 61.
7. J.P. Guo, F.C. Wu, S.R. Xie, L.L. Y and Y.H. Xie, Environmental conditions and exploitation of lead-zinc tailings in Linxiang county, Hunan province, Chinese Journal of Soil Science, 2007, **38**(3), 553.
8. S. Torsten, New insights regarding sound protection with autoclaved aerated concrete, Concrete Precasting Plant and Technology, 2004, **70**(2), 136.
9. A. Hauser and Eggenberger U, Fly ash from cellulose industry as secondary raw material in autoclaved aerated concrete, Cement and Concrete Research, 1999, **29**(3), 297.
10. Z. J. Zhang, C.J. Ke, P.A. Liu and M.F. Zhong, Infrared spectroscopic studies of autoclaved reaction activity of silicious solid waste, J Instrumental Anal. 2010; 29: 68-72.
11. Zhang Z J, Ke C J, Liu P A, Zhong M F. Analysis and mechanism of hydrogarnets formation and transformation in autoclaved reaction, Journal of Instrumental Analysis, 2010, **29**(1), 68.
12. M. Wang, Reaction products of alkali-activated cementing material, Journal of the Chinese Ceramic Society, 2009, **37**(7), 1130.
13. X.F. Tian, D.J. Zhang, H.B. Hou, Z.B. Yang and H. Liu, Microstructure of weak soil stabilization slag cementing material, Journal of the Chinese Ceramic Society, 2006, **34**(5), 636.
14. X.Y. Huang, W. Ni, W.H. Cui, Z.J. Wang and L.P. Zhu, Preparation of autoclaved aerated concrete using copper tailings and blast furnace slag, Construction and Building Materials, 2012, **27**(1), 1.
15. L.Y. Yang, W.H. Wan and J. Li, Research of technological parameter of air-entrained concrete made of phosphorus tailings, Journal of Wuhan University of Technology, 2011, **33**(9), 41.
16. W.Q. Zhang, PhD thesis, Research on preparation and property of tungsten tailings aerated concrete, Nanchang University, China, 2012.
17. J. Chen, T PhD thesis, The preparation and thermal analysisfor B05 autoclaved aerated concrete, Wuhan University of Technology, China, 2009.
18. F.X. Li, Y.Z. Chen and S.Z. Long, Experimental investigation on autoclaved aerated concrete with addition of lead-zinc tailings, Journal of Southwest Jiaotong University, 2008, **43**(6), 810.
19. A.B. Roman, V.M. Victor and V.B. Vladimir, Mechanochemical activation as a tool of increasing catalytic activity, Catalysis Today, 2009, **144**(3-4), 212.
20. V. Sydorchuk, S. Khalameida, V. Zazhigalov, J. Skubiszewska-Zięba and R. Wieczorek-Ciurowa, Influence of mechanochemical activation in various media on structure of porous and non-porous silicas, Applied Surface Science, 2010, **257**(2), 446.
21. S. Osvalda, S. Piero, C. Riccardo, C. Luciano and S. Roberto, Mechanochemical activation of high-carbon fly ash for enhanced carbon reburning, Proceedings of the Combustion Institute, 2011, **33**(2), 2743.
22. Z.L. Yi, H.H. Sun, C. Li, Y.M. Sun and Y. Li, Relationship between polymerization degree and cementitious activity of iron ore tailings, International Journal of Minerals, Metallury and Materials, 2010, **17**(1), 116.
23. Y.C. Zheng, W. Ni, L. Xu, D.Z. Li and J.H. Yang, Mechanochemical activation of iron ore tailings and preparation of high-strength construction materials,

Journal of University of Science and Technology Beijing, 2010, **32**(4), 504.
24.N.R. Buenfeld, Structure and performance of cements, 2nd edition, J. Bensted and P. Barnes, ED. Spon Press, 2002.
25. Л.И. Воженов, Technology of autoclave materials, C.G, TT, Q.D. ED. China Architecture& Building Press, 1985.
26.B.K. You, F.Y. Chen, L.L. Han and H.J. Yan, Investigation of the long-term properties of UEA cement mortar and concrete, Journal of the Chinese Ceramic Society, 2000, **28**(4), 314.
27.P.Y. Yan, J. Peng and X. Qin, Preconditions of the harmful effect induced by delayed ettringite formation in massive shrinkage-compensating concrete, Journal of the Chinese Ceramic Society, 2001, **29**(2), 109.
28.K.L. Scrivener, D. Damidot and Famy C, Possible mechanisms of expansion of concrete exposed to elevated temperatures during curing(also known as DEF) and implications for avoidance of field problems, Cement, Concrete and Aggregates, 1999, **21**(1), 93.
29.N. Zhang, X.M. Liu, H.H. Sun and L.T. Li, Evaluation of blends bauxite-calcination-method red mud with other industrial wastes as a cementitious material: properties and hydration characteristics, Journal of hazardous materials, 2011, **185**(1), 329.
30.M. Singh and M. Grag, Acitvaiton of gypsum anhydrite-slag mixtures, Cement and Concrete Research, 1995, **25**(2), 332.
31.M.D. Li and Y. Qin, The identifieation of phase transition types by differential thermal analysis, Materials Review, 1996(4), 79.
32.D.S. Klimesch and A. Ray, DTA-TGA evaluations of the CaO-Al_2O_3-SiO_2-H_2O system treated hydrothermally, Thermochim Acta, 1999, **334** (1-2),115.
33.X.M. Liu, H.H. Sun, X.P. Feng and N. Zhang, Relationship between the microstructure and reaction performance of aluminosilicate, International Journal of Minerals, Metallurgy and Materials, 2010, **17**(1), 108.

****

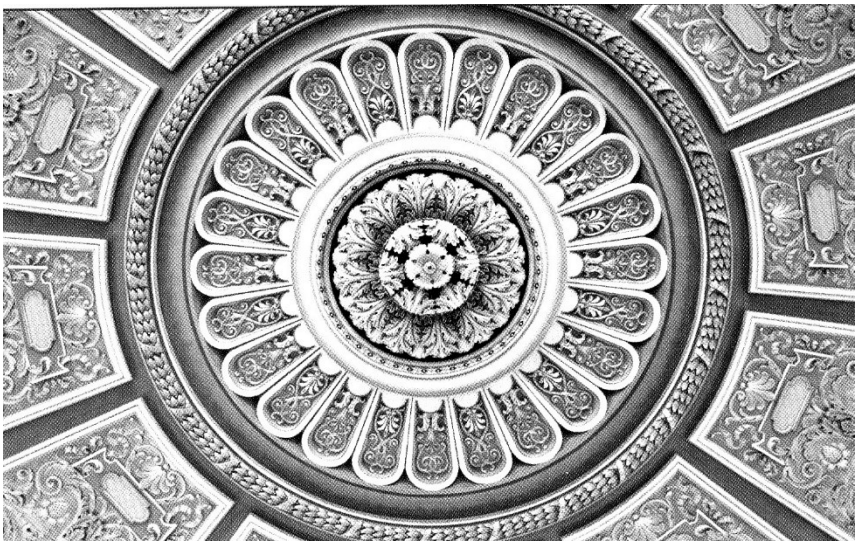

Detaliu plafon (pg. 11 - Nicolae St.Noica - ATENEUL ROMÂN ŞI CONSTRUCTORII SĂI)

Detaliu al plafonului – Sala de concerte a Ateneului Român (pg. 33 - Nicolae St.Noica - ATENEUL ROMÂN ŞI CONSTRUCTORII SĂI)